Electronic coherences in argon through interfering one- and two-photon ionization processes in the vicinity of Feshbach resonances

Roger Y. Bello [1,*] Vicent J. Borràs [1] Jesús González-Vázquez [1] and Fernando Martín [1,2,3]

[1] *Departamento de Química, Módulo 13, Universidad Autónoma de Madrid, 28049 Madrid, Spain*

[2] *Instituto Madrileño de Estudios Avanzados en Nanociencia (IMDEA-Nano), 28049 Madrid, Spain*

[3] *Condensed Matter Physics Center (IFIMAC), Universidad Autónoma de Madrid, 28049 Madrid, Spain*

(Received 27 July 2022; revised 15 September 2022; accepted 23 September 2022; published 14 October 2022)

The role of Rydberg autoionizing states in interfering one- and two-photon ionization paths is theoretically investigated in atomic Ar. The angularly resolved photoionization cross sections for each individual path is provided. By varying the relative optical phase between the two pulses the phase difference between the two interfering paths is extracted. The retrieved phase difference and the photoelectron angular distributions exhibit a strong dependence on the photon energy in the vicinity of the resonant states. In contrast to previous results obtained in atomic Ne, the phase difference features a smooth dependence with photoelectron emission angle.

DOI: 10.1103/PhysRevResearch.4.043028

I. INTRODUCTION

The development of new attosecond light sources has opened the possibility of accessing electron dynamics in atoms and molecules in its natural time scale [1]. In particular, XUV pump-IR probe techniques have been used to access not just the ionization amplitudes but also the phases associated with the scattering states describing the ejected photoelectron. This unfolds the prospect of steering electron and nuclear dynamics, extracting photoionization time delays and even reconstructing electronic wave-packets [2–12]. Currently, two methods are mainly used to retrieve the phases and amplitudes: the streaking technique [13], which combines a single attosecond pump pulse with an infrared probe pulse, and the RABBITT technique [14,15], which combines a train of attosecond pulses with the infrared pulse used to generate them. These two techniques have been successfully applied to investigate atomic systems such as He and Ne [7–9,16–19], and molecular targets such as H_2, NO, and N_2 [10–12,20–25]. An alternative method has been proposed recently for measuring the phases in photoemission [26]. This method combines two phase-locked extreme ultraviolet pulses of frequency ω and 2ω, from a free electron laser. By varying the relative optical phase between the two pulses, the phase difference between the two ionization paths in atomic Ne was measured. In the present work, we apply this technique to theoretically extract the angularly resolved phase difference between the two ionization paths in atomic Ar.

These types of experiments pose a particular challenge for theory. In general, photoionization processes are sensitive to couplings between different ionization channels, including those between energetically open and closed channels. They are also sensitive to electron correlation, as a number of processes involving two or more electrons can also take place, e.g., autoionization of Rydberg states, inner-shell ionization followed by Auger decay, ionization leaving the remaining ion in an excited state (shake-up), Auger decay with shake-up, etc. Correlation in the ion states and interchannel coupling are also necessary to correctly describe the angular distribution of the ejected photoelectron. Thus, any comprehensive theoretical description of these processes must treat both electron correlation in the ion states and correlation of the photoelectron with the target electrons. During the last decades, sophisticated methods based on different approximations have been developed to address these requirements, such as the variational Complex-Khon [27,28] method, the multichannel Schwinger configuration interaction method (MCCI) [29,30], the UK Molecular *R*-matrix [31,32], and the XCHEM approach [33–36]. In particular, the XCHEM method combines standard quantum chemistry techniques for the calculation of highly correlated bound states with a single-center hybrid Gaussian-Bspline basis (GABS) [37] for the description of the electronic continuum. This combination makes XCHEM particularly suited to investigate resonant photoionization processes in many-electron systems. In previous works, XCHEM has been used to accurately describe the photoionization spectra of the He and Ne [33,38] atoms, and small diatomic molecules such as N_2, O_2, and more recently CO [34–36,39].

In the present paper, we take advantage of the XCHEM capabilities to study one- and two-color ω-2ω photoionization of atomic Ar. As illustrated in Fig. 1, one-photon ionization (2ω) leads to an odd final total symmetry, while two-photon ionization (ω) requires an even final total symmetry. In comparison to other atomic systems, such as He or Ne, Ar presents a much richer and complex spectrum (see Fig. 1). The first excited

*roger.bello@uam.es

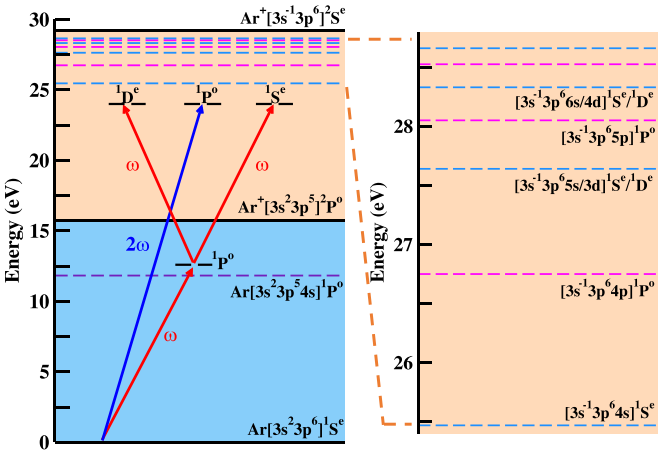

FIG. 1. Schematic representation of the Ar energy levels and ionization thresholds accessible through one- and two-photon transitions. Inset depicts the different photoionization paths. Red and blue arrows represent transitions by ω and 2ω photons, respectively. Final symmetries for each ionization path are also shown.

state of the Ar^+ ($3s^{-1}\ ^2S^e$) cation lies at 29.23 eV, just under twice the energy of the Ar^+ ($3p^5\ ^2P^o$) ground state, which lies at 15.76 eV. Consequently, different Rydberg series converging to the first and second ionization thresholds overlap in this energy region [40] (see Fig. 1). Furthermore, in this same region, two-photon ionization can be resonantly enhanced by the presence of the lowest $^1P^o$ excited state of neutral Ar, which can also leave its trace in the interference between the two ionization paths. In the present work, the effect of both this intermediate $^1P^o$ state and the autoionizing Rydberg states on the angularly resolved one- and two-color photoelectron spectra is discussed. In addition, the angularly resolved phase difference between the two ionization paths is extracted. We find a strong dependence with the photon energy of both the photoelectron angular distributions (PADs) and the phase difference between the one- and two-photon ionization paths in the vicinity of each Rydberg and intermediate-state resonances. In contrast to Ne, where a strong dependence of the phase difference with the photoelectron ejection angle was measured [26], here a smoother dependence is observed. Furthermore, we observe that off resonance, there is a negligible dependence of the phase difference on the photon energy.

The outline of this paper is as follows. In Sec. II we describe the theoretical framework and methodology of the calculations. In Sec. III we explore details of how resonant, bound, and autoionizing states reveal themselves in the features of the anisotropy parameters and angular distributions. In Sec. IV we summarize our specific findings and the prospects for application of this technique to molecular systems.

II. THEORETICAL FRAMEWORK

The photoionization amplitudes for one- and two-photon absorption are obtained within the first- and second-order time-dependent perturbation theory, respectively. For two-photon absorption the ionization amplitude can be formally written as,

$$c_\omega = \sum_k v_{fk} v_{ki} \int_{-\infty}^{\infty} \int_{-\infty}^{t_1} A(t_1) A(t_2) \times e^{i\omega_{ki} t_2} e^{i\omega_{fk} t_1} dt_2 dt_1, \tag{1}$$

where $v_{ij} = \langle \psi_i(\mathbf{r}) | \hat{\mu} | \psi_j(\mathbf{r}) \rangle$ and $\omega_{ij} = E_i - E_j$ are the dipole transition element and energy difference between the i and j states, respectively. A Gaussian envelope was used for the vector potential,

$$A(t) = \frac{A_0}{2} e^{(i\omega t - at^2 - i\phi)}, \tag{2}$$

where ω is the central frequency, ϕ is carrier-envelope phase (CEP), $a = \ln 16/T^2$, T is temporal full-width-at-half-maximum (FWHM), and A_0 is the peak vector potential. The sum in Eq. (1) runs over all intermediate bound and continuum states. Using Gaussian pulses allows the time integral in Eq. (1) to be performed analytically, leading to a simple expression for the ionization amplitude (within the rotating wave approximation),

$$c_\omega = \frac{\pi A_0^2}{8a} \sum_k v_{fk} v_{ki} e^{-\zeta_t^2/8a} w\left(\frac{\Delta}{\sqrt{8a}}\right) e^{-2i\phi_1}, \tag{3}$$

where $\zeta_t = E_f - E_i - 2\omega$, $\Delta = \omega_{fk} - \omega_{ki}$ and $w(x)$ is the *Fadeeva* function [41]. The corresponding one-photon ionization amplitude can be written as

$$c_{2\omega} = \int_{-\infty}^{\infty} v_{fi} A(t) e^{i\omega_{fi} t} dt. \tag{4}$$

Following a similar procedure, one arrives to the expression for the one-photon amplitude:

$$c_{2\omega} = -i \sqrt{\frac{A_0^2 \pi}{4a}} v_{fi} e^{-\xi_n^2/4a - i\phi_2}, \tag{5}$$

where $\xi_n = E_f - E_i - 2\omega$.

Then, the total ionization amplitude can be calculated as a coherent superposition of both ionization paths:

$$I = |c_{2\omega} + c_\omega|^2. \tag{6}$$

The photoelectron angular distribution is given by [42,43]

$$I(\theta) = I_0 \left[1 + \sum_k \beta_k P_k(\cos\theta) \right], \tag{7}$$

where θ is photoelectron emission angle with respect to the light polarization vector, I_0 is the photoionization probability, and β_k are the anisotropy parameters. For one- or two-photon absorption only the terms $k = 2$ or $k = 2, 4$ contribute to the sum, in Eq. (7), respectively. For a combination of one- and two-photon ionization paths, contributions from $k = 1$ up to $k = 4$ have to be considered. The ionization probability, in turn, can be written in terms of the amplitudes and phases of the ionization paths, and the optical phase $\phi = \phi_2 - 2\phi_1$ [26],

$$\begin{aligned} I(\theta, \phi) &= |c_\omega|^2 + |c_{2\omega}|^2 + 2|c_\omega||c_{2\omega}| \cos(\phi - \Delta\eta) \\ &= A + B\cos(\phi - \Delta\eta), \end{aligned} \tag{8}$$

where $\Delta\eta = \eta_\omega - \eta_{2\omega}$ is the phase of the two-photon ionization relative to that of the single-photon ionization.

A. Computational details

The state energies and dipole couplings between bound-bound, bound-continuum, and continuum-continuum states have been calculated using the XCHEM approach [33]. This approach has been explained in detail elsewhere [33–36], so only the computational details will be given here. The initial set of orbitals used in XCHEM calculations are the Ar ($^1S^e$) ground state natural orbitals. The ground state was obtained from a complete active space configuration interaction (CAS-CI) calculation, where the active space included the first four s, three p, and one d orbitals, with the $1s$, $2s$, and $2p$ core orbitals always doubly occupied. These orbitals were obtained from state-average Restricted Active Space SCF (SA-RASSCF) calculation using MOLCAS [44] where they form the active space and in which two $^1S^e$ states were included in the state average. The one-electron basis set was aug-cc-pVTZ basis [45,46]. The ion target states were computed by constructing the (N-1)-electron configuration state functions (CSFs) using the same orbitals used in the MOLCAS calculations of the neutral target states. In the close-coupling calculation, all channels associated with the three components of $^2P^o$ state of the cation (energetically open) and the $^2S^e$ state of the cation (closed channel) were included.

The set of monocentric GABS basis functions [37] used to describe the photoelectron is placed at the system origin, with the B-splines being nonzero for radii $r > R_0$ and the monocentric Gaussians being nonzero for a radii $r < R_1$ such that $R_0 \leqslant R_1$. The B-splines part of the basis consists of a set of 1000 B-splines of order $k = 7$ extending from $R_0 = 10\,\mathrm{a_0}$ up to $R_{\max} = 500\,\mathrm{a_0}$ with $\ell \leqslant 6$. The Gaussian part contains a set of 22 even tempered functions $G_i^M(r) \propto r^{2\zeta+\ell} e^{-\alpha_i r^2}$, with $\alpha_i = \alpha_0 \beta^i$ ($\alpha_0 = 0.01$, $\beta = 1.46$, $i = 0, 1, \ldots, 21$) and $\zeta = 0$, $\ell \leqslant 6$.

In this paper we have considered intensities of $I_{2\omega}$=10^9 Wcm^{-2} and I_{ω}=10^{12} Wcm^{-2} for the 2ω and ω fields, respectively. These intensities are typical in the ω-2ω XFEL experiments [26,47–49]. It is important to point out that neither the absolute intensities nor the relative intensity of the fields affect in any way the phases $\Delta\eta$. Both fields are linearly polarized with a temporal FWHM of T=10 fs. The use of such long pulses guarantees that the PADs and phases will not change significantly with the pulse duration and the results could be extended to longer pulses [50,51]. Only the relative phase $\phi = \phi_2 - 2\phi_1$ is relevant to the observables, we thus set ϕ_1=0. The sum over intermediate states in Eq. (3) includes all bound states whose dipole coupling with the ground state is larger than 10^{-8} a.u., adding up to 61 bound states. The integral over continuum intermediate states is performed over a discrete grid of continuum wave functions [30]. In these calculations the energy grid consisted of 2000 points evenly spaced in energy with spacing $\Delta\varepsilon = 5.5 \times 10^{-4}$ a.u. Additional calculations were performed using a variety of energy grids, for example, a Gauss-Legendre quadrature grid as well as an evenly spaced in momentum grid, all producing the same results. Further increasing the number of either bound or continuum intermediate states did not change the results for photon energies in the region of interest.

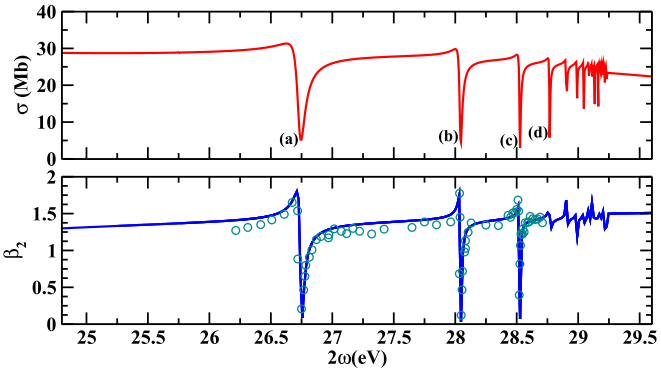

FIG. 2. Cross section and photoelectron angular distribution asymmetry parameter β_2 for single-photon ionization as a function of the photon energy. Insets identify different final resonant Rydberg states converging to the $^2S^e$ ionic state: (a) $3s3p^54p$, (b) $3s3p^55p$, (c) $3s3p^56p$, and (d) $3s3p^57p$. Dark-cyan circles are experimental results from [53]. The experimental results have been shifted in energy by 0.12, 0.05, and 0.01 eV for the first, second, and third resonance, respectively.

III. RESULTS AND DISCUSSION

The ω-2ω interferometric technique probes the phase difference between the one- and two-photon ionization paths, we thus start by analyzing each path individually. The upper panel of Fig. 2 depicts the total photoionization cross-section for one-photon absorption from the $3p^6(^1S^e)$ ground state, leading to states of $^1P^o$ symmetry, for photon energies between the first and second ionization thresholds. The lower panel shows the corresponding β_2 asymmetry parameter. The photoionization cross section is characterized by several autoionizing states associated with the $3s3p^6np$ Rydberg series, converging to the $^2S^e$ state of the ion (see Fig. 1).

Our results are generally in good agreement with those reported previously including measurements using synchrotron radiation and R-matrix calculations [52,53]. As no shift in energy has been applied to the data, the positions of the autoionizing Rydberg states are slightly shifted to higher photon energies when compared to experimental results reported in Ref. [53]. Examination of the partial cross sections (not shown here) suggests that the $3p \rightarrow \varepsilon s$ channel dominates in the vicinity of the resonances, while the $3p \rightarrow \varepsilon d$ channel becomes the prominent channel elsewhere [52]. This behavior is well reflected in the photoelectron angular distributions as photoemission is nearly isotropic, $\beta_2 \sim 0$, near the minimum of each Fano structure where the s channel dominates, rapidly changing to larger values, $\beta_2 \sim 1.25$, away from the resonances where the d channel is dominant. The rapid variations with the photon energy of the β_2 values are well represented in the calculations, hence, the relative amplitude and phase between the s and d channels is accurately described.

Fig. 3 shows the total ionization probability and the angular asymmetry parameters, β_2 and β_4, resulting from a two-photon absorption from the $^1S^e$ ground state, leading to final states of $^1D^e$ or $^1S^e$ symmetry. Results show a qualitative agreement with those presented in Refs. [54–57] obtained using time-independent perturbation theory. However there

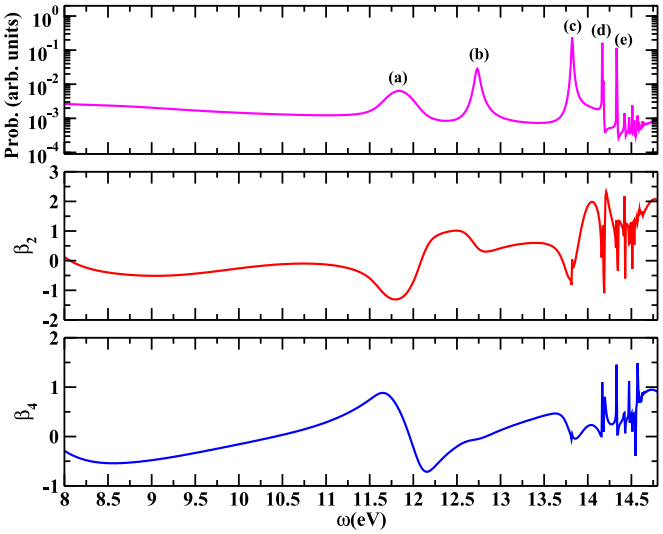

FIG. 3. Total ionization probability (upper panel) and photoelectron angular distribution asymmetry parameters β_2 (middle panel) and β_4 (lower panel) for two-photon absorption as a function of the photon energy. Insets identify different, intermediate or final, resonant states: (a) $4s\,^1P^o$, (b) $4s\,^1S^e$, (c) $3d\,^1D^e$ /$5s\,^1S^e$, (d) $4d\,^1D^e$ /$6s\,^1S^e$, and (e) $5d\,^1D^e$ /$7s\,^1S^e$.

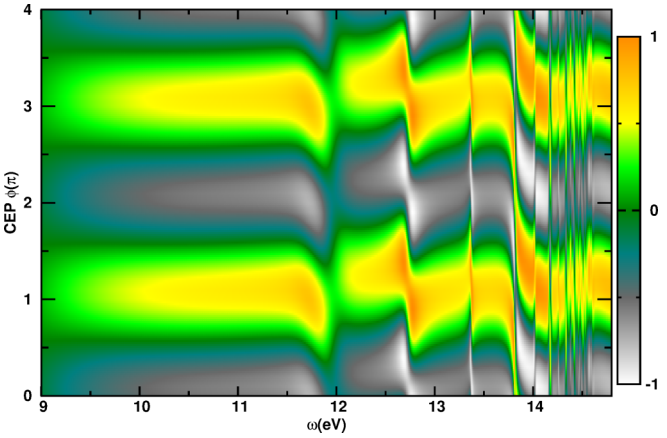

FIG. 4. Photoelectron asymmetry parameter A^e as defined in Eq. (10) as a function of the CEP and photon energy.

are some distinct differences. The ionization probability (upper panel) exhibits a collection of structures that can be attributed to either intermediate or final resonant states. At approximately 11.8 eV a single-photon resonance, due to the intermediate $3s^23p^54s(^1P^o)$ state, is observed. At higher photon energies, the spectrum is dominated by two series of autoionizing Rydberg resonances. These resonances are correlated to two-photon ionization states belonging to the $3s3p^6ns$ ($^1S^e$) and $3s3p^6nd$ ($^1D^e$) series converging to the $^2S^e$ ionic state [40]. These series of Rydberg states have not been included in previous calculations for two-photon ionization angularly resolved cross sections of Ar [54–57]. The first of the autoionizing resonances appears approximately at ∼12.75 eV ($4s\ ^1S^e$). The features labeled (c) and (d) lying at ∼13.8 eV and ∼14.3 eV, respectively, correspond each to two, *ns* and *nd*, overlapping resonances. Above this energy the density of resonances increases significantly, making it difficult to identify the different resonances associated to each series. The effect of these autoionizing states on the photoelectron angular distribution is significant. The β_2 and β_4 parameters dramatically change as the photon energy crosses their energy position. A similar effect was recently reported, using VUV radiation, in molecular nitrogen [58], where a strong variation in the electron emission patterns on the photoelectron energy was recorded. This variation was attributed to the excitation and decay of dipole-forbidden autoionizing Rydberg states. In contrast, the $4s(^1S^e)$ Rydberg state appearing at 12.75 eV, produces a shallow minimum in the β_2 parameter and its effect is barely visible in β_4. We attribute this behavior to the larger width of this specific resonance with respect to the other Rydberg states. The next single-photon resonance appears around 14.0 eV and produces a broad peak in the asymmetry parameters, despite its effect in the ionization probability is nearly imperceptible. In this case, labeling the specific states is practically impossible as the pulse is broad enough to enclose contributions from the $5s(^1P^o)$ and $3d(^1P^o)$ excited states.

We turn our attention now to the interferences of the one- (2ω) and two-photon (ω) ionization paths. While such interferences are not visible in the angle integrated cross sections, they can be observed on the photoelectron angular distributions. The degree of interference between the one- and two-photon ionization paths can be quantified by means of the electron asymmetry parameter A^e, defined as the difference between the electron yields at θ and $\pi - \theta$,

$$A^e(\theta) = \frac{I(\theta) - I(\pi - \theta)}{I(\theta) + I(\pi - \theta)}, \tag{9}$$

where $I(\theta)$ is the probability of the photoelectron being ejected at θ degrees with respect to the light polarization vector [see Eq. (8)]. In particular, for $\theta = 0°$, A^e can be written in terms of the anisotropy parameters β_k [59],

$$A^e(0°) = \frac{\beta_1 + \beta_3}{1 + \beta_2 + \beta_4}. \tag{10}$$

Figure 4 shows the electron asymmetry parameter $A^e(0°)$ as a function of the CEP (ϕ) and the photon energy. The asymmetry is the consequence of the two-path interference 2ω-ω (see Fig. 1), leading to a coherent superposition of the $^1P^o$, $^1S^e$, and $^1D^e$ continua, thus breaking the inversion symmetry of the photoelectron angular distribution [26,48,49,59,60]. The sign of $A^e(0°)$ indicates the angle in which the photoelectron is preferentially ejected. A value of zero indicates an equal photoelectron flux at $\theta = 0°$ and $\theta = 180°$. In some cases, the degree of asymmetry is remarkable, so that the photoelectron is mainly ejected either to the left or to the right. For a given photon energy, this extreme directionality in the photoelectron ejection direction varies cosinusoidally with the CEP (ϕ) [48,61–63]. Such periodicity reflects the interferences between the two quantum paths, leading to states of the same energy but different symmetry. In addition, the asymmetry changes abruptly as the photon energy crosses the energy position of a resonant state. The asymmetry parameter was found to present a similar behavior near a resonant state in H and He atoms and more recently in the H_2 molecule [59,64–66]. These sharp variations result from the phase jump

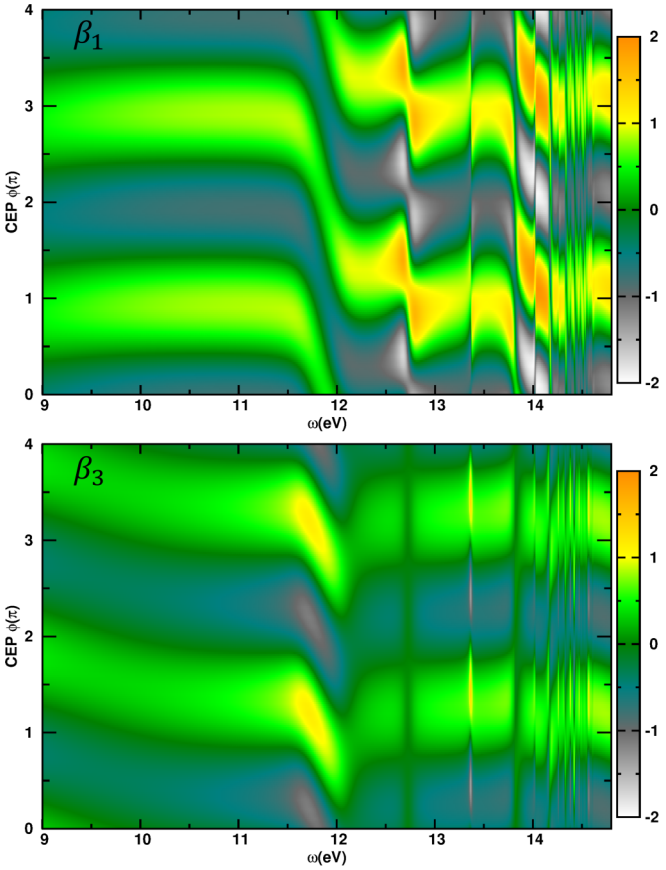

FIG. 5. Photoelectron angular-distribution asymmetry parameters, β_1 (upper panel) and β_3 (lower panel), as a function of the CEP and the photon energy.

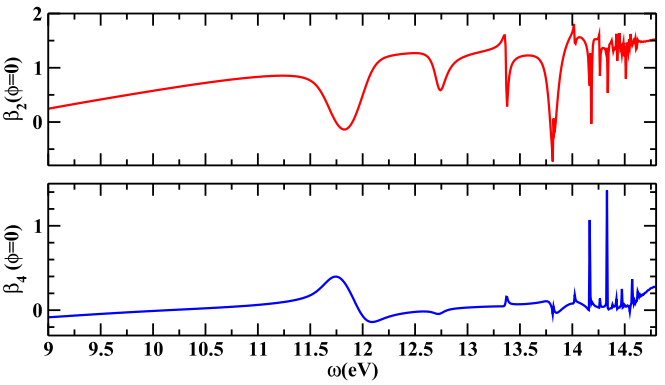

FIG. 6. Photoelectron angular distribution asymmetry parameters, β_2 (upper panel) and β_4 (lower panel), at a fixed CEP ϕ=0 as a function of the photon energy.

experienced by the continuum wave function describing the photoelectron at the resonances energy. As observed in Fig. 4, the periodicity with the CEP exhibited by $A^e(0^\circ)$ is invariable regardless of the photon energy. The spectral width of the resonant structures is independent of the CEP. At each resonance, the ionization amplitude is dominated by a single partial wave. Thus, one would expect the asymmetry to be zero, or at least close to it, at the resonance energy. While this appears to be the case for the $4s(^1P^o)$ resonance at 11.8 eV, the opposite is true for the rest of the resonances.

In order to better understand the features observed in the asymmetry parameter (Fig. 4), in particular the sharp variations experienced around resonant states, we examined its components individually. Figure 5 shows the β_1 (upper panel) and β_3 (lower panel) asymmetry parameters as a function of the CEP (ϕ) and the photon energy. In the perturbative regime the values of β_2 and β_4 are independent of the CEP ϕ [26,48,49,59,67]. Accordingly, in Fig. 6 we only present the values of β_2 and β_4 as a function of the photon energy at a fixed CEP $\phi = 0$. As expected from Fig. 4, the anisotropy parameters, depicted in Figs. 5 and 6, exhibit strong variations as a function of the photon energy, as observed previously in Figs. 2 and 3. This further underlines the effect of the resonant states on the PADs, as the resonant states appearing in each of the possible final symmetries $^1P^o$, $^1S^e$, and $^1D^e$, are now taken into account. Although the β_1 and β_3 oscillate with the same periodicity, there is a distinct phase shift between them. This is due to the fact that the different partial waves, associated to each final symmetry, contribute in different ways to the anisotropy parameters [59].

For completeness, Fig. 7 shows the PADs as a function of the CEP (ϕ) at different photon energies, clockwise from the upper left, 11.0, 11.8, 12.0, and 13.0 eV. For each photon energy the PAD features the same oscillations with the CEP observed previously in Figs. 4 and 5. Two of these photon energies, 11.0 and 13 eV, have been chosen to be well off resonance (see for instance Fig. 6), while 11.8 and 12.0 eV lie at the extremes of the $4s(^1P^o)$ resonance structure. The PADs at 11.0 and 13.0 eV are highly asymmetric, exhibiting a major photoelectron emission at $\theta \sim 0$ or $\theta \sim \pi$, while minor differences are observed between the two energies. In contrast, the PADs at 11.8 and 12.0 eV feature a more complex structure, signature of the interference between different partial waves correlated to different continua, *i.e.,* $(s,d)\,^1P^o$, $(p)\,^1S^e$, and $(p,f)\,^1D^e$. The variation experienced by the PAD in just 0.2 eV, from 11.8 to 12.0 eV, is noteworthy. Additionally, there is a phase difference between electrons emitted at $\theta \sim \pi/2$ and $\theta \sim 0$, i.e., $\Delta\eta(\pi/2) \neq \Delta\eta(0)$ [see Eq. (8)]. In particular the phase difference is apparent at 11.8 and 12.0 eV, where it can reach large values $\sim\pi/2$. Note that the PADs at θ and $\pi - \theta$ oscillate in antiphase that is $\Delta\eta(\pi-\theta) = \Delta\eta(\theta) + \pi$.

Finally, for each photoelectron energy the phase difference between the one- and two-photon paths can be extracted by fitting the PADs to Eq. (8). This was recently carried out in Ref. [26], where the authors were able to determine, both theoretically and experimentally, such phase difference in Ne. In Fig. 8 we present the phase difference $\Delta\eta$ as a function of the photon energy for different photoelectron emission angles. The phase difference features the same sudden variations previously observed in Figs. 4–6 in the vicinity of a resonance. In some cases, for instance at the $\sim$13.75 eV $3d\,^1D^e/5s\,^1S^e$ resonances, an almost full $\sim\pi$ jump is observed. In contrast, off resonance, *i.e.,* for photon energies below 11.5 eV, $\Delta\eta$ experiences small changes with the photon energy, varying only over $\sim 0.1\pi$ in absolute value. In contrast to the results reported in Ne [26] where the angle-resolved phase exhibited a strong dependence on the photoelectron emission angle, here a smoother dependence is observed. As already observed in

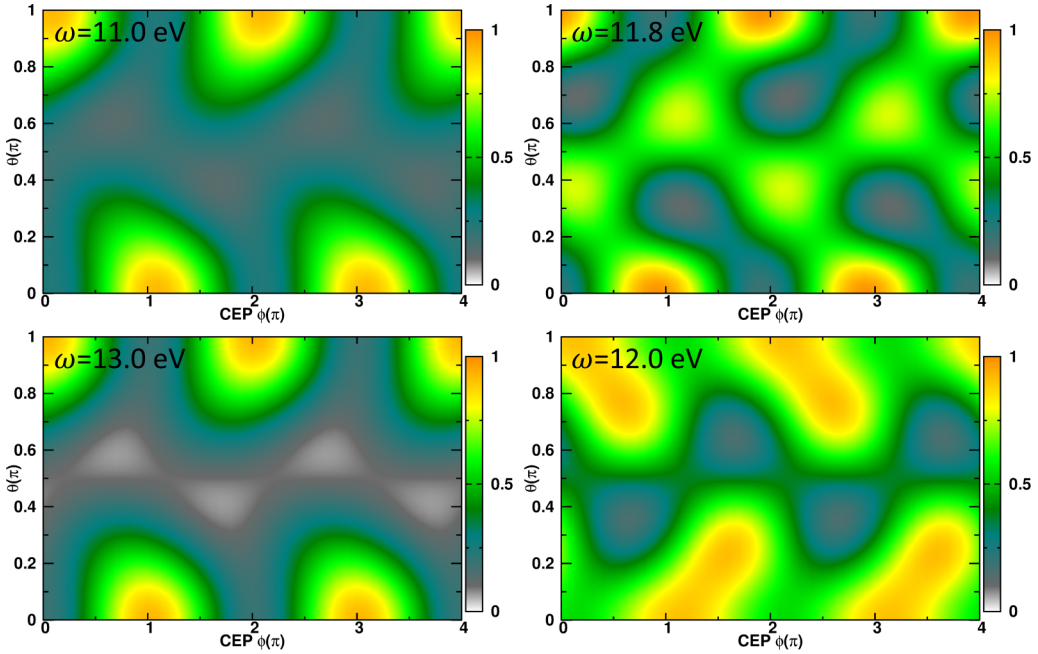

FIG. 7. Photoelectron angular distribution as a function of the CEP for photoelectron energies of (clockwise from the upper left) 11.0, 11.8, 12.0, and 13.0 eV.

Fig. 7, only in the vicinity of the intermediate $4s\,^1P^o$ resonance a large $\Delta\eta(75^\circ) - \Delta\eta(0^\circ) \sim \pi/2$ is observed. The analysis of the partial ionization probabilities (see Fig. 9) shows that the εd channel dominates off resonance. In contrast, in the vicinity of the $4s\,^1P^o$ resonance the combination of the εp and εd channels is dominant, while in the vicinity of the $4s\,^1S^e$ and $3d\,^1D^e$ /$5s\,^1S^e$ resonances only the εp channel contributes significantly. In general, when photoionization is governed by a single partial wave, one can expect a rather weak dependence of the phase with the photoelectron emission angle. The larger angular dependence of the phase variation previously reported in Ne [26] is mainly due to the fact that several partial ionization probabilities have comparable magnitude in the off-resonance region. Indeed, as shown in Ref. [68], the εf channel also has a significant contribution and, in fact, it can even be dominant. The importance of the εf channel in two-photon ionization of Ne was also pointed out in an earlier work [69]. The different behavior in Ne and Ar is likely due to the absence of a radial node in the $2p$ orbitals (Ne) and the presence of one in the $3p$ orbitals (Ar) from which the electrons are ejected, despite the fact that the angular momentum is the same in both cases ($\ell = 1$).

It can be observed that around 11.91 eV, i.e., in the vicinity of the $4s\,^1P^o$ resonance, the calculated relative phase does not change with the emission angle (see Fig. 8). However, a closer inspection of the results in this energy region shows that the different curves do not intercept each other exactly at the same energy. This quasi-perfect isotropy of the relative phases is due to an accidental cancellation of the phases associated with the εp and εd partial waves at around 11.91 eV, as a consequence of the rapid and pronounced variation of the εp amplitude in this energy region while the εd amplitude remains practically constant (see the corresponding probabilities in Fig. 9).

In two-photon processes (ω) the probability ratio and phase difference between $^1S^e$ and $^1D^e$ continua can be derived from the β_2 and β_4 parameters [50,51,70]. However ω-2ω measurements do not provide direct access to individual phase differences between the $^1P^o$, $^1S^e$, and $^1D^e$ continua (see Ref. [26,67]). They can be used in tandem with two-photon

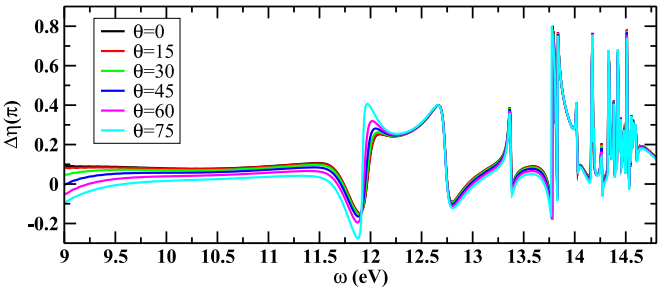

FIG. 8. Phase difference between the one- and two-photon ionization paths as a function of the photon energy for different photoelectron emission angles.

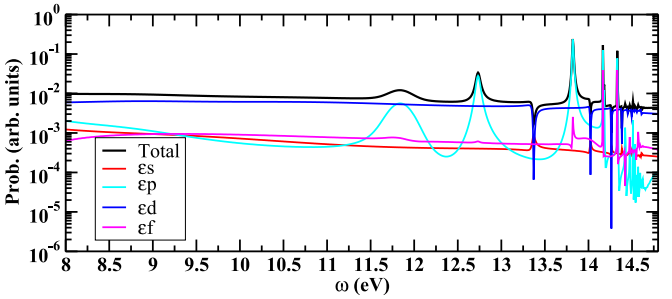

FIG. 9. Total and partial ionization probabilities for ω-2ω absorption as a function of the photon energy.

measurements, to provide a complete picture of the photoionization process. This difficulty can be circumvented in the energy regions where a single channel dominates, for instance in the vicinity of a resonance.

IV. CONCLUSION

In the present work, we have studied the interference between one- and two-photon processes in atomic Ar in the presence of intermediate-state resonances and Rydberg autoionizing states. We have reported angularly resolved photoionization probabilities for one- and two-photon absorption individually. The photoelectron angular distributions and the phase difference between the two ionization paths exhibit a complex behavior with the photon energy, a consequence of the numerous resonant states contributing to the photoelectron spectrum. In contrast to previous experiments performed in Ne, the phase difference features a rather small dependence with the photoelectron emission angle. These results demonstrate the importance of using correlated methods in the presence of autoionizing states, an expected scenario in many-electron systems. The present calculations can serve as a benchmark for future pump-probe experiments in atomic Ar, specifically those aiming to study energy- and angle-resolved atomic time delays in the presence of Rydberg states.

It is worth pointing out that the information extracted using this method is complementary to that obtained from streaking and RABBITT methods. Indeed, thanks to the intensity and wavelength tunability of the free-electron laser this method can be extended to study valence as well as inner shell photoionization in atomic and molecular systems. Additionally, in RABBIT, the intensity of the IR pulse has to be, on the one hand, low enough to avoid the absorption or the emission of more than one IR photon that could overlap with transition involving different ionization channels and, on the other hand, sufficiently high to make these transitions visible. This can pose a problem for systems where the different ionization channels lie very close in energy to each other, e.g., in molecules. In the present ω-2ω scheme, this problem would be minimized since the photon energies are much larger than the energy separation between different ionization thresholds.

ACKNOWLEDGMENTS

All calculations were performed at the Mare Nostrum Supercomputer of the Red Española de Supercomputación (BSC-RES) and the Centro de Computación Científica de la Universidad Autónoma de Madrid (CCC-UAM). Work supported by the Synergy Grant of the European Research Council TOMATTO, the MICINN Project No. PID2019-105458RB-I00, the Comunidad de Madrid project FULMATEN (Ref. Y2018NMT-5028), the "Severo Ochoa" Programme for Centres of Excellence in R&D (CEX2020-001039-S), and the "María de Maeztu" Programme for Units of Excellence in R&D (CEX2018-000805-M). R.Y.B. acknowledges support from the Project No. IJC2020-045659 financed by the MCIN/AEI/10.13039/501100011033 and by EU NextGenerationEU/PRTR. V.J.B. thanks the MICINN for the FPI Grant No. (BES-2017-081521) related to the Project No. FIS2016-77889-R.

[1] M. Nisoli, P. Decleva, F. Calegari, A. Palacios, and F. Martín, Attosecond electron dynamics in molecules, Chem. Rev. **117**, 10760 (2017).

[2] A. S. Kheifets and I. A. Ivanov, Delay in Atomic Photoionization, Phys. Rev. Lett. **105**, 233002 (2010).

[3] D. Guénot, K. Klünder, C. L. Arnold, D. Kroon, J. M. Dahlström, M. Miranda, T. Fordell, M. Gisselbrecht, P. Johnsson, J. Mauritsson, E. Lindroth, A. Maquet, R. Taïeb, A. L'Huillier, and A. S. Kheifets, Photoemission-time-delay measurements and calculations close to the 3*s*-ionization-cross-section minimum in ar, Phys. Rev. A **85**, 053424 (2012).

[4] J. M. Dahlström, D. Guénot, K. Klünder, M. Gisselbrecht, J. Mauritsson, A. L'Huillier, A. Maquet, and R. Taïeb, Theory of attosecond delays in laser-assisted photoionization, Chem. Phys. **414**, 53 (2013), attosecond spectroscopy.

[5] R. Pazourek, S. Nagele, and J. Burgdörfer, Time-resolved photoemission on the attosecond scale: Opportunities and challenges, Faraday Discuss. **163**, 353 (2013).

[6] R. Pazourek, S. Nagele, and J. Burgdörfer, Attosecond chronoscopy of photoemission, Rev. Mod. Phys. **87**, 765 (2015).

[7] V. Gruson, L. Barreau, Á. Jiménez-Galan, F. Risoud, J. Caillat, A. Maquet, B. Carré, F. Lepetit, J.-F. Hergott, T. Ruchon, L. Argenti, R. Taïeb, F. Martín, and P. Salieres, Attosecond dynamics through a fano resonance: Monitoring the birth of a photoelectron, Science **354**, 734 (2016).

[8] S. Heuser, Á. Jiménez Galán, C. Cirelli, C. Marante, M. Sabbar, R. Boge, M. Lucchini, L. Gallmann, I. Ivanov, A. S. Kheifets, J. M. Dahlström, E. Lindroth, L. Argenti, F. Martín, and U. Keller, Angular dependence of photoemission time delay in helium, Phys. Rev. A **94**, 063409 (2016).

[9] C. Cirelli, C. Marante, S. Heuser, C. L. M. Petersson, Á. J. Galán, L. Argenti, S. Zhong, D. Busto, M. Isinger, S. Nandi, S. Maclot, L. Rading, P. Johnsson, M. Gisselbrecht, M. Lucchini, L. Gallmann, J. M. Dahlström, E. Lindroth, A. L'Huillier, F. Martín *et al.*, Anisotropic photoemission time delays close to a fano resonance, Nat. Commun. **9**, 955 (2018).

[10] L. Cattaneo, J. Vos, R. Y. Bello, A. Palacios, S. Heuser, L. Pedrelli, M. Lucchini, C. Cirelli, F. Martín, and U. Keller, Attosecond coupled electron and nuclear dynamics in dissociative ionization of H_2, Nat. Phys. **14**, 733 (2018).

[11] X. Gong, W. Jiang, J. Tong, J. Qiang, P. Lu, H. Ni, R. Lucchese, K. Ueda, and J. Wu, Asymmetric Attosecond Photoionization in Molecular Shape Resonance, Phys. Rev. X **12**, 011002 (2022).

[12] L. Cattaneo, L. Pedrelli, R. Y. Bello, A. Palacios, P. D. Keathley, F. Martín, and U. Keller, Isolating Attosecond Electron Dynamics in Molecules where Nuclei Move Fast, Phys. Rev. Lett. **128**, 063001 (2022).

[13] J. Itatani, F. Quéré, G. L. Yudin, M. Yu. Ivanov, F. Krausz, and P. B. Corkum, Attosecond Streak Camera, Phys. Rev. Lett. **88**, 173903 (2002).

[14] V. Véniard, R. Taïeb, and A. Maquet, Phase dependence of (n+1)-color (n>1) ir-uv photoionization of atoms with higher harmonics, Phys. Rev. A **54**, 721 (1996).

[15] P. M. Paul, E. S. Toma, P. Breger, G. Mullot, F. Augé, Ph. Balcou, H. G. Muller, and P. Agostini, Observation of a train of attosecond pulses from high harmonic generation, Science **292**, 1689 (2001).

[16] M. Swoboda, T. Fordell, K. Klünder, J. M. Dahlström, M. Miranda, C. Buth, K. J. Schafer, J. Mauritsson, A. L'Huillier, and M. Gisselbrecht, Phase Measurement of Resonant Two-Photon Ionization in Helium, Phys. Rev. Lett. **104**, 103003 (2010).

[17] C. Palatchi, J. M. Dahlström, A. S. Kheifets, I. A. Ivanov, D. M. Canaday, P. Agostini, and L. F. DiMauro, Atomic delay in helium, neon, argon and krypton, J. Phys. B: At. Mol. Opt. Phys. **47**, 245003 (2014).

[18] D. Guénot, D. Kroon, E. Balogh, E. W. Larsen, M. Kotur, M. Miranda, T. Fordell, P. Johnsson, J. Mauritsson, M. Gisselbrecht, K. Varjù, C. L. Arnold, T. Carette, A. S. Kheifets, E. Lindroth, A. L'Huillier, and J. M. Dahlström, Measurements of relative photoemission time delays in noble gas atoms, J. Phys. B: At. Mol. Opt. Phys. **47**, 245602 (2014).

[19] L. Barreau, C. L. M. Petersson, M. Klinker, A. Camper, C. Marante, T. Gorman, D. Kiesewetter, L. Argenti, P. Agostini, J. González-Vázquez, P. Salières, L. F. DiMauro, and F. Martín, Disentangling Spectral Phases of Interfering Autoionizing States from Attosecond Interferometric Measurements, Phys. Rev. Lett. **122**, 253203 (2019).

[20] S. Haessler, B. Fabre, J. Higuet, J. Caillat, T. Ruchon, P. Breger, B. Carré, E. Constant, A. Maquet, E. Mével, P. Salières, R. Taïeb, and Y. Mairesse, Phase-resolved attosecond near-threshold photoionization of molecular nitrogen, Phys. Rev. A **80**, 011404 (2009).

[21] M. Huppert, I. Jordan, D. Baykusheva, A. von Conta, and H. J. Wörner, Attosecond Delays in Molecular Photoionization, Phys. Rev. Lett. **117**, 093001 (2016).

[22] J. Vos, L. Cattaneo, S. Patchkovskii, T. Zimmermann, C. Cirelli, M. Lucchini, A. Kheifets, A. S. Landsman, and U. Keller, Orientation-dependent stereo wigner time delay and electron localization in a small molecule, Science **360**, 1326 (2018).

[23] S. Nandi, E. Plésiat, S. Zhong, A. Palacios, D. Busto, M. Isinger, L. Neoričić, C. L. Arnold, R. J. Squibb, R. Feifel, P. Decleva, A. L'Huillier, F. Martín, and M. Gisselbrecht, Attosecond timing of electron emission from a molecular shape resonance, Sci. Adv. **6**, eaba7762 (2020).

[24] S. Heck, D. Baykusheva, M. Han, J.-B. Ji, C. Perry, X. Gong, and H. J. Wörner, Attosecond interferometry of shape resonances in the recoil frame of CF_4, Sci. Adv. **7**, eabj8121 (2021).

[25] H. Ahmadi, E. Plésiat, M. Moioli, F. Frassetto, L. Poletto, P. Decleva, C. D. Schröter, T. Pfeifer, R. Moshammer, A. Palacios, F. Martin, and G. Sansone, Attosecond photoionisation time delays reveal the anisotropy of the molecular potential in the recoil frame, Nat. Commun. **13**, 1242 (2022).

[26] D. You, K. Ueda, E. V. Gryzlova, A. N. Grum-Grzhimailo, M. M. Popova, E. I. Staroselskaya, O. Tugs, Y. Orimo, T. Sato, K. L. Ishikawa, P. A. Carpeggiani, T. Csizmadia, M. Füle, G. Sansone, P. Kumar Maroju, A. D'Elia, T. Mazza, M. Meyer, C. Callegari, M. Di Fraia *et al.*, New Method for Measuring Angle-Resolved Phases in Photoemission, Phys. Rev. X **10**, 031070 (2020).

[27] B. I. Schneider and T. N. Rescigno, Complex kohn variational method: Application to low-energy electron-molecule collisions, Phys. Rev. A **37**, 3749 (1988).

[28] C. W. McCurdy and T. N. Rescigno, Collisions of electrons with polyatomic molecules: Electron-methane scattering by the complex kohn variational method, Phys. Rev. A **39**, 4487 (1989).

[29] R. E. Stratmann and R. R. Lucchese, A graphical unitary group approach to study multiplet specific multichannel electron correlation effects in the photoionization of O_2, J. Chem. Phys. **102**, 8493 (1995).

[30] R. Y. Bello, R. R. Lucchese, T. N. Rescigno, and C. W. McCurdy, Correlated variational treatment of ionization coupled to nuclear motion: Ultrafast pump and ionizing probe of electronic and nuclear dynamics in lih, Phys. Rev. Res. **3**, 013228 (2021).

[31] J. M. Carr, P. G. Galiatsatos, J. D. Gorfinkiel, A. G. Harvey, M. A. Lysaght, D. Madden, Z. Mašín, M. Plummer, J. Tennyson, and H. N. Varambhia, Ukrmol: a low-energy electron- and positron-molecule scattering suite, Eur. Phys. J. D **66**, 58 (2012).

[32] L. R. Moore, M. A. Lysaght, L. A. A. Nikolopoulos, J. S. Parker, H. W. van der Hart, and K. T. Taylor, The rmt method for many-electron atomic systems in intense short-pulse laser light, J. Mod. Opt. **58**, 1132 (2011).

[33] C. Marante, M. Klinker, I. Corral, J. González-Vázquez, L. Argenti, and F. Martín, Hybrid-basis close-coupling interface to quantum chemistry packages for the treatment of ionization problems, J. Chem. Theory Comput. **13**, 499 (2017).

[34] M. Klinker, C. Marante, L. Argenti, J. González-Vázquez, and F. Martín, Electron correlation in the ionization continuum of molecules: Photoionization of N_2 in the vicinity of the hopfield series of autoionizing states, J. Phys. Chem. Lett. **9**, 756 (2018).

[35] M. Klinker, C. Marante, L. Argenti, J. González-Vázquez, and F. Martín, Partial cross sections and interfering resonances in photoionization of molecular nitrogen, Phys. Rev. A **98**, 033413 (2018).

[36] S. Marggi Poullain, M. Klinker, J. González-Vázquez, and F. Martín, Resonant photoionization of O_2 up to the fourth ionization threshold, Phys. Chem. Chem. Phys. **21**, 16497 (2019).

[37] C. Marante, L. Argenti, and F. Martín, Hybrid gaussian–*b*-spline basis for the electronic continuum: Photoionization of atomic hydrogen, Phys. Rev. A **90**, 012506 (2014).

[38] C. Marante, M. Klinker, T. Kjellsson, E. Lindroth, J. González-Vázquez, L. Argenti, and F. Martín, Photoionization using the xchem approach: Total and partial cross sections of ne and resonance parameters above the $2s^2 2p^5$ threshold, Phys. Rev. A **96**, 022507 (2017).

[39] V. J. Borrás, J. González-Vázquez, L. Argenti, and F. Martín, Molecular-frame photoelectron angular distributions of co in the vicinity of feshbach resonances: An xchem approach, J. Chem. Theory Comput. **17**, 6330 (2021).

[40] C. McKenna and H. W. van der Hart, Multiphoton ionization cross sections of neon and argon, J. Phys. B: At. Mol. Opt. Phys. **37**, 457 (2004).

[41] M. Abramowitz and I. A. Stegun, *Handbook of Mathematical Functions with Formulas, Graphs, and Mathematical Tables* (US Government printing office, 1964), Vol. 55.

[42] J. C. Tully, R. S. Berry, and B. J. Dalton, Angular distribution of molecular photoelectrons, Phys. Rev. **176**, 95 (1968).

[43] E. Arnous, S. Klarsfeld, and S. Wane, Angular distribution in the two-quantum atomic photoeffect, Phys. Rev. A **7**, 1559 (1973).

[44] F. Aquilante, J. Autschbach, R. K. Carlson, L. F. Chibotaru, M. G. Delcey, L. De Vico, I. Fdez. Galván, N. Ferré, L. M. Frutos, L. Gagliardi, M. Garavelli, A. Giussani, C. E. Hoyer, G. Li Manni, H. Lischka, D. Ma, P. A. Malmqvist, T. Muller, A. Nenov, M. Olivucci *et al.*, Molcas 8: New capabilities for multiconfigurational quantum chemical calculations across the periodic table, J. Comput. Chem. **37**, 506 (2016).

[45] T. H. Dunning, Gaussian basis sets for use in correlated molecular calculations. i. the atoms boron through neon and hydrogen, J. Chem. Phys. **90**, 1007 (1989).

[46] R. A. Kendall, T. H. Dunning, and R. J. Harrison, Electron affinities of the first-row atoms revisited. systematic basis sets and wave functions, J. Chem. Phys. **96**, 6796 (1992).

[47] F. Holzmeier, R. Y. Bello, M. Hervé, A. Achner, T. M. Baumann, M. Meyer, P. Finetti, M. Di Fraia, D. Gauthier, E. Roussel, O. Plekan, R. Richter, K. C. Prince, C. Callegari, H. Bachau, A. Palacios, F. Martín, and D. Dowek, Control of H_2 Dissociative Ionization in the Nonlinear Regime using Vacuum Ultraviolet Free-Electron Laser Pulses, Phys. Rev. Lett. **121**, 103002 (2018).

[48] K. C. Prince, E. Allaria, C. Callegari, R. Cucini, G. De Ninno, S. Di Mitri, B. Diviacco, E. Ferrari, P. Finetti, D. Gauthier, L. Giannessi, N. Mahne, G. Penco, O. Plekan, L. Raimondi, P. Rebernik, E. Roussel, C. Svetina, M. Trovò, M. Zangrando *et al.*, Coherent control with a short-wavelength free-electron laser, Nat. Photonics **10**, 176 (2016).

[49] M. Di Fraia, O. Plekan, C. Callegari, K. C. Prince, L. Giannessi, E. Allaria, L. Badano, G. De Ninno, M. Trovò, B. Diviacco, D. Gauthier, N. Mirian, G. Penco, P. R. Ribič, S. Spampinati, C. Spezzani, G. Gaio, Y. Orimo, O. Tugs, T. Sato *et al.*, Complete Characterization of Phase and Amplitude of Bichromatic Extreme Ultraviolet Light, Phys. Rev. Lett. **123**, 213904 (2019).

[50] K. L. Ishikawa and K. Ueda, Competition of Resonant and Nonresonant Paths in Resonance-Enhanced Two-Photon Single Ionization of He by an Ultrashort Extreme-Ultraviolet Pulse, Phys. Rev. Lett. **108**, 033003 (2012).

[51] K. L. Ishikawa and K. Ueda, Photoelectron angular distribution and phase in two-photon single ionization of h and he by a femtosecond and attosecond extreme-ultraviolet pulse, Appl. Sci. **3**, 189 (2013).

[52] T. Carette, J. M. Dahlström, L. Argenti, and E. Lindroth, Multiconfigurational hartree-fock close-coupling ansatz: Application to the argon photoionization cross section and delays, Phys. Rev. A **87**, 023420 (2013).

[53] N. Berrah, B. Langer, J. Bozek, T. W. Gorczyca, O. Hemmers, D. W. Lindle, and O. Toader, Angular-distribution parameters andR-matrix calculations of ar resonances, J. Phys. B: At. Mol. Opt. Phys. **29**, 5351 (1996).

[54] A. F. Starace and T.-F. Jiang, Transition-matrix theory for two-photon ionization of rare-gas atoms and isoelectronic ions with application to argon, Phys. Rev. A **36**, 1705 (1987).

[55] C. Pan, B. Gao, and A. F. Starace, Two-photon ionization of the ar atom and detachment of the f^- ion, Phys. Rev. A **41**, 6271 (1990).

[56] C. Pan and A. F. Starace, Angular distribution of electrons following two-photon ionization of the ar atom and two-photon detachment of the f^- ion, Phys. Rev. A **44**, 324 (1991).

[57] I. D. Petrov, B. M. Lagutin, V. L. Sukhorukov, A. Knie, and A. Ehresmann, Correlation and polarization effects in two-photon photoionization of Ar, Phys. Rev. A **93**, 033408 (2016).

[58] K. A. Larsen, R. Y. Bello, R. R. Lucchese, T. N. Rescigno, C. W. McCurdy, D. S. Slaughter, and T. Weber, Role of dipole-forbidden autoionizing resonances in nonresonant one-color two-photon single ionization of N_2, Phys. Rev. A **102**, 063118 (2020).

[59] A. N. Grum-Grzhimailo, E. V. Gryzlova, E. I. Staroselskaya, J. Venzke, and K. Bartschat, Interfering one-photon and two-photon ionization by femtosecond vuv pulses in the region of an intermediate resonance, Phys. Rev. A **91**, 063418 (2015).

[60] Y.-Y. Yin, C. Chen, D. S. Elliott, and A. V. Smith, Asymmetric Photoelectron Angular Distributions from Interfering Photoionization Processes, Phys. Rev. Lett. **69**, 2353 (1992).

[61] G. G. Paulus, F. Lindner, H. Walther, A. Baltuška, E. Goulielmakis, M. Lezius, and F. Krausz, Measurement of the Phase of Few-Cycle Laser Pulses, Phys. Rev. Lett. **91**, 253004 (2003).

[62] M. J Abel, T. Pfeifer, A. Jullien, P. M. Nagel, M. J. Bell, D. M. Neumark, and S. R. Leone, Carrier-envelope phase-dependent quantum interferences in multiphoton ionization, J. Phys. B: At. Mol. Opt. Phys. **42**, 075601 (2009).

[63] S. Fukahori, T. Ando, S. Miura, R. Kanya, K. Yamanouchi, T. Rathje, and G. G. Paulus, Determination of the absolute carrier-envelope phase by angle-resolved photoelectron spectra of ar by intense circularly polarized few-cycle pulses, Phys. Rev. A **95**, 053410 (2017).

[64] N. Douguet, A. N. Grum-Grzhimailo, E. V. Gryzlova, E. I. Staroselskaya, J. Venzke, and K. Bartschat, Photoelectron angular distributions in bichromatic atomic ionization induced by circularly polarized vuv femtosecond pulses, Phys. Rev. A **93**, 033402 (2016).

[65] Y. Wang and C. H. Greene, Resonant control of photoelectron directionality by interfering one- and two-photon pathways, Phys. Rev. A **103**, 053118 (2021).

[66] R. Y. Bello, F. Martín, and A. Palacios, Attosecond laser control of photoelectron angular distributions in xuv-induced ionization of h2, Faraday Discuss. **228**, 378 (2021).

[67] Y. Orimo, O. Tugs, T. Sato, D. You, K. Ueda, and K. L. Ishikawa, Interferometric extraction of photoionization-path amplitudes and phases from time-dependent multiconfiguration self-consistent-field simulations, J. Phys. B: At. Mol. Opt. Phys. **54**, 074001 (2021).

[68] E. V. Gryzlova, A. N. Grum-Grzhimailo, E. I. Staroselskaya, N. Douguet, and K. Bartschat, Quantum coherent control of the photoelectron angular distribution in bichromatic-field ionization of atomic neon, Phys. Rev. A **97**, 013420 (2018).

[69] R. Moccia, N. K. Rahman, and A. Rizzo, Two-photon ionisation cross section calculations of noble gases: results for Ne and Ar, J. Phys. B **16**, 2737 (1983).

[70] L. H. Haber, B. Doughty, and S. R. Leone, Continuum phase shifts and partial cross sections for photoionization from excited states of atomic helium measured by high-order harmonic optical pump-probe velocity map imaging, Phys. Rev. A **79**, 031401(R) (2009).